

Broadband optical waveguide couplers with arbitrary coupling ratios designed using a genetic algorithm

Po-Han Fu,¹ Yi-Chou Tu,¹ and Ding-Wei Huang^{1,2,*}

¹Graduate Institute of Photonics and Optoelectronics, National Taiwan University, Taipei 10617, Taiwan

²Department of Electrical Engineering, National Taiwan University, Taipei 10617, Taiwan

*dwhuang@ntu.edu.tw

Abstract: In this work, we present a generalized design of broadband optical waveguide couplers with arbitrary coupling ratios on the silicon-on-insulator platform. The device is segmented into 34 short sections, where the propagation constant and the coupling coefficient of each section are viewed as variables during the optimization process. The optimal variable combination is determined by a genetic algorithm. We can achieve a performance superior to that of other design methods with fewer degrees of freedom. For 75%/25%, 50%/50%, 25%/75%, and 0%/100% couplers, the device lengths are 34 μm and the $\pm 2\%$ bandwidths are all in excess of 100 nm at the central wavelength of 1580 nm.

© 2016 Optical Society of America

OCIS codes: (060.1810) Buffers, couplers, routers, switches, and multiplexers; (130.2790) Guided waves; (130.3120) Integrated optics devices.

References and links

1. L. Chen and Y. Chen, "Compact, low-loss and low-power 8 \times 8 broadband silicon optical switch," *Opt. Express* **20**, 18977–18985 (2012).
2. J. Campenhout, W. Green, S. Assefa, and Y. Vlasov, "Low-power, 2 \times 2 silicon electro-optic switch with 110-nm bandwidth for broadband reconfigurable optical networks," *Opt. Express* **17**, 24020–24029 (2009).
3. X. Jiang, J. Wu, Y. Yang, T. Pan, J. Mao, B. Liu, R. Liu, Y. Zhang, C. Qiu, C. Tremblay, and Y. Su, "Wavelength and bandwidth-tunable silicon comb filter based on Sagnac loop mirrors with Mach-Zehnder interferometer couplers," *Opt. Express* **24**, 2183–2188 (2016).
4. H. Yu, D. Korn, M. Pantouvaki, J. Van Campenhout, K. Komorowska, P. Verheyen, G. Lepage, P. Absil, D. Hillerkuss, L. Alloatti, J. Leuthold, R. Baets, and W. Bogaerts, "Using carrier-depletion silicon modulators for optical power monitoring," *Opt. Lett.* **37**, 4681–4683 (2012).
5. D. Miller, "Designing linear optical components," *Opt. Photon. News* **24**, 38–38 (2013).
6. C. Chen, X. Zhu, Y. Liu, K. Wen, M. Chik, T. Baehr-Jones, M. Hochberg and K. Bergman, "Programmable dynamically-controlled silicon photonic switch fabric," *J. Lightw. Technol.* **34**, 2952–2958 (2016).
7. W. Huang, "Coupled-mode theory for optical waveguides: an overview," *J. Opt. Soc. Am. A* **11**, 963–983 (1994).
8. A. Takagi, K. Jinguiji and M. Kawachi, "Broadband silica-based optical waveguide coupler with asymmetric structure," *Electron. Lett.* **26**, 132–133, (1990).
9. A. Takagi, K. Jinguiji and M. Kawachi, "Wavelength characteristics of (2 \times 2) optical channel-type directional couplers with symmetric or nonsymmetric coupling structures," *J. Lightwave Technol.* **10**, 735–746 (1992).
10. Z. Lu, H. Yun, Y. Wang, Z. Chen, F. Zhang, N. Jaeger, and L. Chrostowski, "Broadband silicon photonic directional coupler using asymmetric-waveguide based phase control," *Opt. Express* **23**, 3795–3808 (2015).
11. S. Tseng, "Robust coupled-waveguide devices using shortcuts to adiabaticity," *Opt. Lett.* **39**, 6600–6603 (2014).
12. X. Chen, R. Wen, and S. Tseng, "Analysis of optical directional couplers using shortcuts to adiabaticity," *Opt. Express* **24**, 18322–18331 (2016).
13. A. Maese-Novo, R. Halir, S. Romero-García, D. Pérez-Galacho, L. Zavargo-Peché, A. Ortega-Moñux, I. Molina-Fernández, J. Wangüemert-Pérez, and P. Cheben, "Wavelength independent multimode interference coupler," *Opt. Express* **21**, 7033–7040 (2013).
14. C. R. Doerr, M. Cappuzzo, E. Chen, A. Wong-Foy, L. Gomez, A. Griffin, and L. Buhl, "Bending of a planar lightwave circuit 2 \times 2 coupler to desensitize it to wavelength, polarization, and fabrication changes," *IEEE Photon. Technol. Lett.* **17**, 1211–1213 (2005).
15. H. Morino, T. Maruyama and K. Iiyama, "Reduction of wavelength dependence of coupling characteristics using Si optical waveguide curved directional coupler," *J. Lightwave Technol.* **32**, 2188–2192 (2014).
16. S. Chen, Y. Shi, S. He, and D. Dai, "Low-loss and broadband 2 \times 2 silicon thermo-optic Mach-Zehnder switch with bent directional couplers," *Opt. Lett.* **41**, 836–839 (2016).

17. Y. Wang, Z. Lu, M. Ma, H. Yun, F. Zhang, N. A. F. Jaeger, and L. Chrostowski, "Compact broadband directional couplers using subwavelength gratings," *IEEE Photon. J.* **8**, 7101408 (2016).
18. Z. Michalewicz, *Genetic Algorithms + Data Structures = Evolution Programs*, 2nd ed. (Springer-Verlag, 1994).
19. L. Sanchis, A. Häkansson, D. Lopez-Zanón, J. Bravo-Abad and J. Sánchez-Dehesa, "Integrated optical devices design by genetic algorithm," *Appl. Phys. Lett.* **84**, 4460–4462 (2004).
20. A. Häkansson and J. Sánchez-Dehesa, "Inverse designed photonic crystal de-multiplex waveguide coupler," *Opt. Express* **13**, 5440–5449 (2005).
21. A. Häkansson, P. Sanchis, J. Sánchez-Dehesa and J. Martí, "High-efficiency defect-based photonic-crystal tapers designed by a genetic algorithm," in *J. Lightw. Technol.* **23**, 3881–3888 (2005).
22. D. Correia, J. da Silva and H. Hernandez-Figueroa, "Genetic algorithm and finite-element design of short single-section passive polarization converter," *IEEE Photon. Technol. Lett.* **15**, 915–917 (2003).
23. F. Bahrami, M. Maisonneuve, M. Meunier, J. Aitchison, and M. Mojahedi, "[An improved refractive index sensor based on genetic optimization of plasmon waveguide resonance](#)," *Opt. Express* **21**, 20863–20872 (2013).
24. A. Liu, R. Wu, and Y. Lin, "A compact design of W-band high-pass waveguide filter using genetic algorithms and full-wave finite element analysis," *IEICE T. Electron.* **E88-C**, 1764–1771 (2005).
25. J. Marqués-Hueso, L. Sanchis, B. Cluzel, F. de Fornel, and J. P. Martínez-Pastor, "Genetic algorithm designed silicon integrated photonic lens operating at 1550 nm," *Appl. Phys. Lett.* **97**, 071115 (2010).
26. S. Chuang, *Physics of Optoelectronic Devices* (Wiley, 2009).
27. Comsol Multiphysics, <https://www.comsol.com/>.
28. Q. Deng, L. Liu, X. Li, and Z. Zhou, "Strip-slot waveguide mode converter based on symmetric multimode interference," *Opt. Lett.* **39**, 5665–5668 (2014).
29. P. Vanbrabant, J. Beeckman, K. Neyts, R. James, and F. Fernandez, "A finite element beam propagation method for simulation of liquid crystal devices," *Opt. Express* **17**, 10895–10909 (2009).
30. H. Li, "Refractive index of silicon and germanium and its wavelength and temperature derivatives," *J. Phys. Chem. Ref. Data* **9**, 561–658 (1993).
31. I. Malitson, "Interspecimen comparison of the refractive index of fused silica," *J. Opt. Soc. Am.* **55**, 1205–1208 (1965).
32. MATLAB Global Optimization Toolbox, Genetic Algorithm Options, <http://www.mathworks.com/help/gads/genetic-algorithm-options.html>.
33. Lumerical Solutions, Inc., <https://www.lumerical.com>
34. P. Fu, T. Chiang, N. Cheng, Y. Ma, and D. Huang, "Microring resonator composed of vertical slot waveguides with minimum polarization mode dispersion over a wide spectral range," *Appl. Opt.* **55**, 3626–3631 (2016).

1. Introduction

Optical waveguide couplers are one of the most essential building blocks in photonic integrated circuits (PICs) which are commonly used in Mach-Zehnder interferometer-based devices such as N by N optical switches [1, 2], filters [3], and power monitors [4–6]. To increase operating bandwidths, the responses of such devices are required to be wavelength insensitive, especially over the C + L band (the spectral range for $\lambda = 1530 – 1630$ nm) for practical uses. Therefore, a precise and broadband optical waveguide coupler is needed. Conventional directional couplers, which consist of two parallel waveguides, have been widely used in PICs owing to their compactness and integrability on the silicon-on-insulator (SOI) platform. Based on the coupled mode theory (CMT), the normalized coupled optical power has the form $\sin^2(\kappa L_T)$, where κ is the coupling coefficient and L_T is the total propagation length [7]. However, κ is inherently highly sensitive to the wavelength, and thus operating bandwidths are extremely limited.

Studies have shown that the wavelength dependency of an optically coupled system can be reduced by utilizing asymmetric couplers [8–10], adiabatic couplers [11, 12], multi-mode interference couplers [13], bent couplers [14–16], couplers with phase control sections [10], and couplers with sub-wavelength gratings [13, 17]. All of the aforementioned methods enhance the operating bandwidths by applying specific functions to the waveguide geometry, and hence the propagation constants β , and κ over a wide spectral range can be determined. Therefore, it is reasonable to deduce that the precision and operating bandwidth may be further enhanced by implementing a generalized design where the whole system is segmented into N short sections, and the values of β and κ of each section can be arbitrary, which are eventually determined by an optimization process. However, relative approaches with regard to the design of broadband optical waveguide couplers have not been discussed to date.

Genetic algorithm (GA) is an optimization technique based on the process of natural selection, which is highly efficient in dealing with a problem with a large set of variables for which the solution search space is not well understood [18]. In the last decade, GAs have been widely used for the design of waveguide devices including spot size converters [19], photonic-crystal-based couplers [20] and tapers [21], polarization converters [22], sensors [23], filters [24], and photonic lens [25]. In this study, a GA is used for the generalized design of broadband optical waveguide couplers for arbitrary coupling ratios in the SOI platform. A lookup table of the propagation constants and coupling coefficients for a wide variety of variable combinations is constructed and therefore the spectral response of the system can be analyzed by the CMT [7, 26] during the optimization process. The optimal design is further verified by using the beam envelope method (BEM) [27]. The results indicate a good agreement with the CMT. For the wavelength range $\lambda = 1530 - 1630$ nm (C + L band), the coupling ratios are nearly wavelength-independent for 75%/25%, 50%/50%, 25%/75%, and 0%/100% couplers.

2. System analysis

2.1. Waveguide properties

Figure 1 shows the schematic of an optically coupled system in general view with the coordinate axes labeled at the bottom right. z_i denotes the position of the i th joint in the z -axis. The system consists of two SOI strip waveguides, labeled WG0 and WG1, respectively. Light is launched into the input port of WG0 and exits from the bar and the cross ports. Due to the limitation of wafer preparation, the waveguide heights h are kept constant. As the light beam propagates in the z -direction, the gap G between WG0 and WG1 and the waveguide widths, w_0 and w_1 are functions of z . Or equivalently, the propagation constants of WG0 and WG1, which are denoted as β_0 and β_1 , respectively, are functions of z . The distances between the central line $x = 0$ to the edges of WG0 and WG1 are both equal to $G/2$.

Each strip waveguide enables two guided modes with major components E_x and E_y of the electric field, which are typically defined as quasi-TE and -TM modes. Note that the design in connection with quasi-TE and -TM modes can be achieved separately by the same method. Here we take the quasi-TM mode as an example in the discussion.

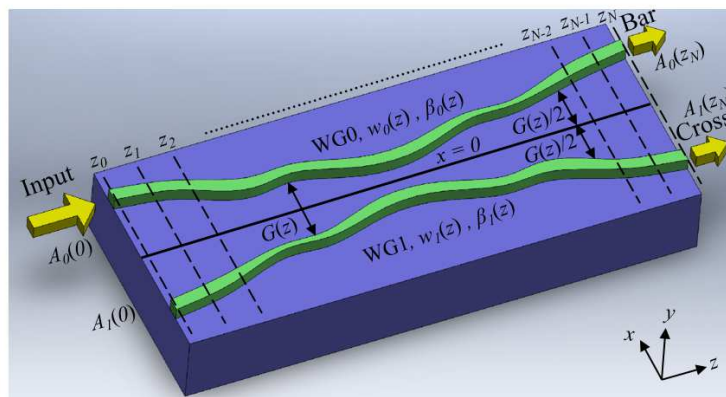


Fig. 1. Schematic of an optically coupled system in general view.

Studies have reported that the system can be solved numerically by the beam propagation method [11, 12], finite-difference time-domain method [10, 15], finite element method (FEM) [24, 28], or the finite element beam propagation method (FEBPM) [29], etc. However, these numerical methods require the generation of meshes to approximate the domain geometry, which

may be time consuming in handling cases consisting of a wide variety of variable combinations, especially with optimization cases. To complete the calculation within a reasonable time and with limited computational resources, CMT-based analysis without meshing the geometry can be considered as an alternative approach for the initial optimal design. For an optically coupled system shown in Fig.1, the mode amplitudes of WG0 and WG1 denoted as $A_0(\lambda, z)$ and $A_1(\lambda, z)$, respectively, satisfy the coupled mode equations [26]:

$$\frac{\partial}{\partial z} \begin{bmatrix} A_0(\lambda, z) \\ A_1(\lambda, z) \end{bmatrix} = -j \begin{bmatrix} \bar{\beta}(\lambda, z) + \Delta\beta(\lambda, z) & \kappa(\lambda, z) \\ \kappa(\lambda, z) & \bar{\beta}(\lambda, z) - \Delta\beta(\lambda, z) \end{bmatrix} \begin{bmatrix} A_0(\lambda, z) \\ A_1(\lambda, z) \end{bmatrix}, \quad (1)$$

Suppose $A_0(\lambda, 0)$ and $A_1(\lambda, 0)$ are launched at $z = 0$, the solution is given by:

$$A_0(\lambda, z) = (A_0(\lambda, 0)(\cos(\psi z) - \frac{j\Delta\beta \sin(\psi z)}{\psi}) - A_1(\lambda, 0)\frac{j\kappa \sin(\psi z)}{\psi}))e^{-j\bar{\beta}z}, \quad (2)$$

$$A_1(\lambda, z) = (-A_0(\lambda, 0)\frac{j\kappa \sin(\psi z)}{\psi} + A_1(\lambda, 0)(\cos(\psi z) + \frac{j\Delta\beta \sin(\psi z)}{\psi}))e^{-j\bar{\beta}z}, \quad (3)$$

where $\psi(\lambda, z) = \sqrt{\kappa^2(\lambda, z) + \Delta\beta^2(\lambda, z)}$, $\bar{\beta}(\lambda, z) = (\beta_0(\lambda, z) + \beta_1(\lambda, z))/2$, $\Delta\beta(\lambda, z) = (\beta_0(\lambda, z) - \beta_1(\lambda, z))/2$, and the corresponding waveguide width with regard to the value $\bar{\beta}(\lambda, z)$ is $\bar{w}(\lambda, z)$. It is known that the conventional CMT is accurate only for weakly confined and weakly coupled waveguides, because errors may arise if κ is determined by the overlap integral of the electric fields [26]. In this case, all of the variables required in the coupled mode equations including β_0 , β_1 , κ , and ψ are obtained by solving the eigenvalue problems of a single and coupled waveguides based on the FEM [27], where κ is more accurate compared with the one obtained by the overlap integral [7]. The quasi-TM mode profile (i.e., the normalized E_y , which is the major component of the eigenvector) of a single strip waveguide with width $w_0(w_1)$ and height h of 320 nm is shown in Fig. 2(a). Figures 2(b) and (c) present the mode profiles of the even and odd modes of identical coupled waveguides with $w_0 = w_1 = 320$ nm, $h = 320$ nm, and $G = 300$ nm. Based on the supermode theory, ψ can be determined by the propagation constants of the even mode, β_e , and the odd modes, β_o , where $\psi = (\beta_e - \beta_o)/2$ [7].

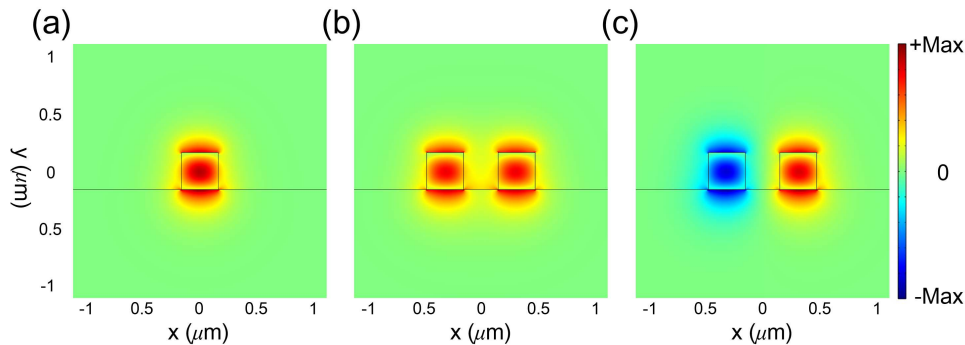


Fig. 2. Mode profiles of the quasi-TM polarization of (a) a single strip waveguide, (b) even and (c) odd modes of coupled waveguides.

By assigning the value of $\bar{\beta}(\lambda, z)$ independently of z (i.e., $\bar{\beta}(\lambda, z) = \bar{\beta}(\lambda)$) with $\bar{w} = 320$ nm, Fig. 3 shows the real value of $\psi = \sqrt{\kappa^2 + \Delta\beta^2}$ and approximated $\psi' = \sqrt{\kappa_0^2 + \Delta\beta^2}$ versus $|\Delta\beta|$ at $\lambda = 1580$ nm and $G = 300$ nm, where κ_0 is the coupling coefficient when $\Delta\beta = 0$. $\psi' \approx \psi$, and thus $\kappa \approx \kappa_0$ for all $|\Delta\beta|$ if $\bar{\beta}(\lambda, z) = \bar{\beta}(\lambda)$, and the result may facilitate the following approximation of κ . Moreover, by the relation $\bar{\beta} = (\beta_0 + \beta_1)/2$, w_1 can be directly acquired

once w_0 is determined, and vice versa. In this way, the number of variables in the optimization process reduces by half compared with the case when $\bar{\beta}$ is dependent on z .

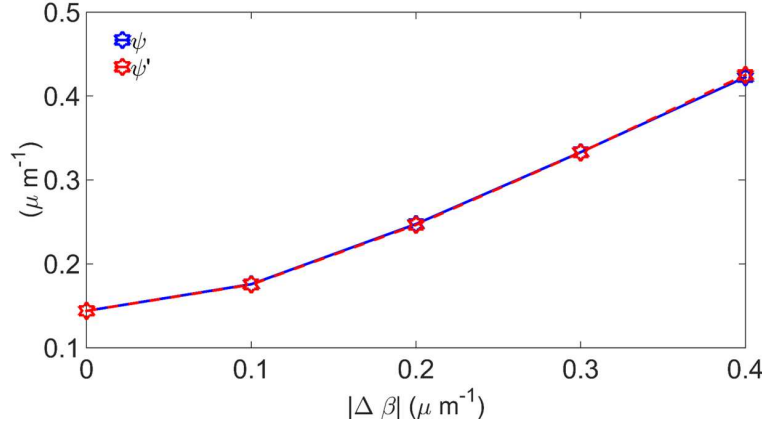


Fig. 3. ψ and ψ' versus $|\Delta\beta|$ at $\lambda = 1580$ nm and $G = 300$ nm.

Based on Eqs. (2) and (3), since the solution of the CMT is independent of $\bar{\beta}$ which only induces identical phase terms for both A_0 and A_1 , here, we let $\bar{\beta}$ be invariant along the z -direction. Before the optimization begins, a lookup table of $\Delta\beta$ and κ should be built in connection with variables, and the values of $\Delta\beta$ and κ required in the following spectral response analysis based on the CMT can be acquired by interpolation according to the lookup table. The variables that determine $\Delta\beta$ and κ are λ , w_0 , w_1 , and G , where $\lambda = 1530\text{--}1630$ nm, w_0 and $w_1 = 280\text{--}360$ nm, and $G = 150$ nm–1 μ m. In this case, the value of \bar{w} is assigned to be 320 nm, $\Delta\beta = \Delta\beta(\lambda, w_0(w_1))$, and $\kappa = \kappa(\lambda, w_0, w_1, G)$. However, it may be cumbersome to construct the lookup table of κ if a four-dimensional variable space is needed. Based on the result shown in Fig. 3, the approximation of κ is made, where $\kappa(\lambda, w_0, w_1, G) \approx \kappa(\lambda, 320\text{nm}, 320\text{nm}, G) = \kappa(\lambda, G)$ for simplification.

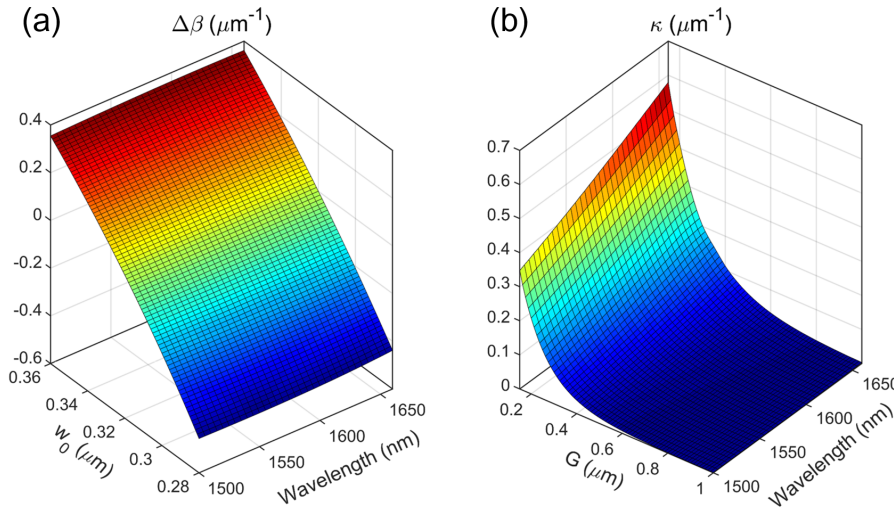


Fig. 4. Plots of lookup tables of (a) $\Delta\beta(\lambda, w)$ and (b) $\kappa(\lambda, G)$ calculated by the FEM.

By considering the material dispersion relation of Si [30] and SiO_2 [31] for the spectral range $\lambda = 1500\text{--}1660\text{ nm}$, Fig. 4(a) shows the plot of the lookup table of $\Delta\beta(\lambda, w_0)$. $\Delta\beta$ increases quadratically as w_0 increases while $\Delta\beta$ remains obscured as λ varies. Thus $\Delta\beta(\lambda, w) \approx \Delta\beta(w)$. On the other hand, the plot of the lookup table of $\kappa(\lambda, G)$ is presented in Fig. 4(b), where κ decreases exponentially as G increases for all λ and increases with increasing λ . All the parameters and variables are defined as follows, and the information shown in Fig. 4 will be implemented in the fitness function of the GA.

2.2. CMT in transfer matrix form

To determine the values of $w_0(z)$, $w_1(z)$ and $G(z)$, the optimization process based on the GA is used, and thus the device is segmented into discrete trapezoidal sections with the length Δz . Each trapezoidal section is approximated by M small rectangles with the length $\Delta z'$, and the total number of small rectangles is N . Figure 5 shows the k th rectangle where $\Delta z' = z'_{k+1} - z'_k$, $z'_k = k\Delta z'$, for $k = 0, 1, \dots, N - 1$. Note that the subscript i denoted in Fig. 1 is $i = \lfloor k/M \rfloor$. The notation of all variables is defined as follows, if X is a function of z , X_k is synonymous with $X(z'_k)$, where X can be A_0 , A_1 , $\Delta\beta$, κ , and ψ . The output of the entire system, including $A_{0,N}$ and $A_{1,N}$, can be determined by solving Eq. (1) with the input amplitudes as the initial condition. However, in this case $\Delta\beta$ and κ are arbitrary, since the variables cannot be separated while solving the differential equations. Hence, a simple form may be needed to facilitate the calculations. If $\Delta\beta$ and κ can be approximated as constants within a short section within $z = z'_k$ and $z = z'_{k+1}$, the coupled mode equations become [26]:

$$\begin{bmatrix} A_{0,k+1} \\ A_{1,k+1} \end{bmatrix} = e^{-j\bar{\beta}\Delta z'} \begin{bmatrix} \cos(\psi_k \Delta z') - \frac{j\Delta\beta_k \sin(\psi_k \Delta z')}{\psi_k} & \frac{-j\kappa_k \sin(\psi_k \Delta z')}{\psi_k} \\ \frac{-j\kappa_k \sin(\psi_k \Delta z')}{\psi_k} & \cos(\psi_k \Delta z') + \frac{j\Delta\beta_k \sin(\psi_k \Delta z')}{\psi_k} \end{bmatrix} \begin{bmatrix} A_{0,k} \\ A_{1,k} \end{bmatrix} \\ = T_k \begin{bmatrix} A_{0,k} \\ A_{1,k} \end{bmatrix}. \quad (4)$$

Eq. (4) has the form $M_{k+1} = T_k M_k$, and thus the output matrix M_N can be evaluated in a convenient way by using $M_N = (\prod_{k=0}^{N-1} T_k) M_0$, where $M_0 = \begin{bmatrix} 1 \\ 0 \end{bmatrix}$ in this case.

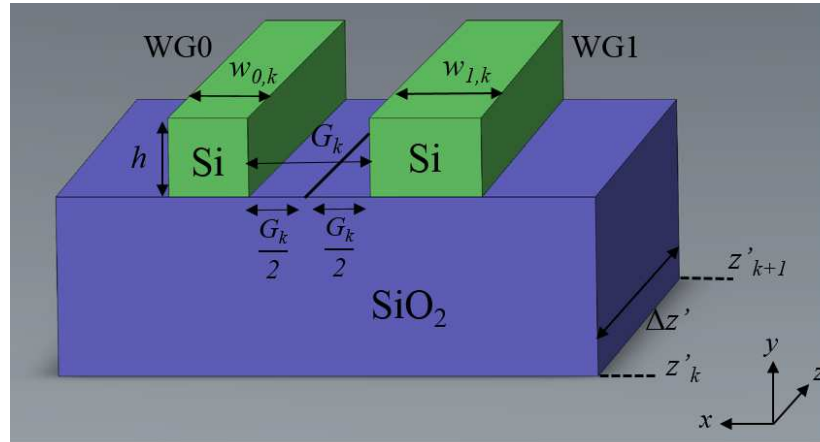


Fig. 5. The k th section of the device.

3. Optimization based on GA

Since the coupling ratio of conventional couplers exhibits the highest sensitivity to λ when the coupling ratio is 50%/50%, here, the design of broadband 50%/50% coupler is chosen as an example. Note that the design of waveguide couplers for arbitrary coupling ratios can be achieved in a similar manner.

Consider an optically coupled system shown in Fig. 1 with a total length $L = 34 \mu\text{m}$. The lengths of fan-in and fan-out regions connected to both ends of the system are $8 \mu\text{m}$, where $w_0 = w_1 = 320 \text{ nm}$, and $G = 1 \mu\text{m}$, and thus κ is negligible ($4.3 \times 10^{-4} - 1.9 \times 10^{-3} \mu\text{m}^{-1}$) from $\lambda = 1530 \text{ nm}$ to 1630 nm according to the lookup table. Considering the fan-in and fan-out regions where $G \geq 1 \mu\text{m}$ is required, abrupt changes of G along the device may occur for a short coupling length (*e.g.*, $L < 20 \mu\text{m}$) and thus the accuracy of the transfer matrix method based on the CMT may be seriously degraded. To ensure the accuracy, a larger coupling length $L = 34 \mu\text{m}$ is chosen. The variables $w_{0,i}$, $w_{1,i}$, and G_i for the waveguide structures are designed by the GA. In this case, the directional coupler is segmented into 34 trapezoidal sections where $\Delta z = 1 \mu\text{m}$, and thus the superscript of z_i means the position of $i \mu\text{m}$ in the z -axis. The number of variables for the optimization process can be determined by the lengths of L and Δz , which may influence the optimized fitness value and difficulty of convergence. In this case $N_s = 34$ and $\Delta z = 1 \mu\text{m}$ is a reasonable starting point for optimization. In order to facilitate the connection for different parts of the system as well as to reduce the complexity for the optimization, G_i is set to be symmetric while $\Delta\beta_i$ is made nearly anti-symmetric to $z = 17 \mu\text{m}$. Therefore $G_{34-i} = G_i$. On the other hand, $w_{1,34-i} = w_{0,i}$ and $w_{0,34-i} = w_{1,i}$, except for $i = 17$. The entire system can be described by a possible solution (individual) \vec{V} that contains a set of variables

$$\vec{V} = [G_1 \quad G_2 \quad \dots \quad G_{17} \quad w_{0,1} \quad w_{0,2} \quad \dots \quad w_{0,17}]^T. \quad (5)$$

During the optimization processes, G_i and $w_{0,i}$ are searched in the intervals $[0.15 \mu\text{m}, 1 \mu\text{m}]$ and $[280 \text{ nm}, 360 \text{ nm}]$, respectively. Moreover, the width variation of the neighboring sections, $|w_{0,i+1} - w_{0,i}|$, is restricted to 10 nm and the deviation angle caused by the variation of G cannot exceed 2.5 degrees as referenced to the z -axis to ensure the accuracy of the CMT. In order to obtain a good accuracy for the transfer matrix calculation after \vec{V} is determined, each trapezoidal section is approximated by ten smaller rectangles (*i.e.*, $M = 10$) with the length $\Delta z' = 0.1 \times \Delta z = 0.1 \mu\text{m}$. Also, the parameters including all w_0 , w_1 , and G are calculated by linear interpolation based on \vec{V} . Thus, $\kappa(\lambda, z)$ and $\beta(\lambda, z)$ for all λ and z can be determined based on the lookup table and the output of the bar and cross ports for all λ can be calculated.

The purpose of the GA is to minimize the deviation of the coupling ratio of the bar port $P_0 = |A_0(L)|^2$ and the cross port $P_1 = |A_1(L)|^2$ from 50% for $\lambda = 1530 - 1630 \text{ nm}$, and thereby the fitness function $F_{50/50}$ can be defined in the form

$$F_{50/50} = \sum_{l=0}^{10} (P_0(\lambda_l) - 0.5)^2, \quad (6)$$

,where $\lambda_l = 1530 + 10 \cdot l \text{ nm}$ for $l = 0, 1, \dots, 10$ and the performance is evaluated by the value of $F_{50/50}$. Note that the CMT used in the fitness function satisfies the power conservation and the total power is normalized to a unity, *i.e.*, $P_0 + P_1 = 1$. Also, the fitness function can be customized for different purposes. Therefore, one can design a directional coupler for arbitrary coupling ratios for a specific spectral range. The GA begins with the emergence of the initial population, which is 300 for each generation. Then the corresponding $F_{50/50}$ for every \vec{V} is calculated, and the selection used is the roulette wheel where the probability to be selected is inversely proportional to its $F_{50/50}$ value. The selected individuals \vec{V}_1 and \vec{V}_2 are one pair of

new parents that can generate their new offspring \vec{V}_{child} by a crossover operator. In this case, the crossover rate is 0.6 and \vec{V}_{child} is created by taking a weighted average of \vec{V}_1 and \vec{V}_2 [32].

$$\vec{V}_{child} = \vec{V}_1 + R(\vec{V}_2 - \vec{V}_1), \quad (7)$$

where R is a random number within the interval [0,1]. Then a small percentage of the variables of the offspring is altered by a mutation operator. The mutation operator enables the GA to escape from the local minimum and to search a broader space.

At first, we have tried the optimization with randomly generated initial populations. However, it is difficult to obtain a satisfactory result for the optimization process due to its tendency to converge to a local minimum. To address this issue, a simplified model for finding the initial population is constructed, where $\kappa(z)$ and $\beta(z)$ at $\lambda = 1580$ nm are expressed for three variables p, q, r as well as two random functions $R_1(z)$ and $R_2(z)$ which independently generate random numbers within the interval [0,1]. Based on previous studies [10, 14–16], largest $\kappa(z)$ usually occurs in the middle of the device thus it is assumed that $\kappa(1580 \text{ nm}, z) = p \cdot z + q \cdot R_1(z)$, and $\Delta\beta(1580 \text{ nm}, z) = r \cdot (R_2(z) - 0.5)$, with $0.01 < p < 0.03$, $0 < q < 0.1$, and $0 < r < 0.8$ for $z = 17 \mu\text{m}$. Once $\kappa(1580 \text{ nm}, z)$ and $\Delta\beta(1580 \text{ nm}, z)$ are determined, $\kappa(\lambda, z)$ and $\Delta\beta(\lambda, z)$ for $\lambda = 1530 - 1630$ nm can be acquired from the lookup table and the spectral response can be calculated. In the simplified model, owing to the fact that an approximated form of κ is assigned based on [10, 14–16], it is easier to obtain a more reasonable result as compared to the unsimplified model without a proper initial population. The optimization process terminates when $F_{50/50} < 0.04$, and the resultant $w_0(z)$, $w_1(z)$, and $G(z)$ serve as the initial population for the succeeding optimization process in the unsimplified model.

Table 1. $w_{0,i}$, $w_{1,i}$, and G_i of the initial and final populations.

i	Initial Population			Final Population		
	$w_{0,i}$ (nm)	$w_{1,i}$ (nm)	G_i (nm)	$w_{0,i}$ (nm)	$w_{1,i}$ (nm)	G_i (nm)
1	348.30	295.70	941.83	309.96	330.67	927.14
2	347.59	296.22	883.15	313.76	326.48	884.69
3	341.13	301.18	814.34	322.91	317.14	814.42
4	332.19	308.61	736.65	329.13	311.33	738.38
5	324.50	315.61	665.36	321.96	318.06	664.88
6	320.15	319.85	598.50	320.00	320.00	599.46
7	318.58	321.43	531.10	317.12	322.93	531.99
8	317.23	322.81	454.37	316.90	323.16	455.44
9	313.35	326.92	395.82	311.81	328.60	396.28
10	306.02	335.21	366.95	306.19	335.01	366.12
11	296.97	346.59	335.68	297.27	346.19	336.48
12	291.00	354.87	317.73	289.77	356.67	317.82
13	295.00	349.25	319.18	287.21	360.49	307.56
14	291.44	354.23	300.45	291.84	353.66	302.00
15	300.03	342.59	233.81	300.05	342.57	235.08
16	309.80	330.84	192.14	310.38	330.19	192.04
17	317.63	322.41	175.41	315.52	324.60	176.91

After choosing a proper initial population, the optimization process deals with the loop containing selection, crossover, and mutation, the optimized value of $F_{50/50}$ is as low as 1.4×10^{-4} and can be obtained after 350 generations. $w_{0,i}$, $w_{1,i}$, and G_i for $i = 1, 2, \dots, 17$ of the initial and final populations are shown in Table 1.

Figure 6 shows the evolution of the best F for the GA, and Fig. 7(a) shows the normalized power output of the bar port, P_0 , and cross port, P_1 , of a broadband 50%/50% coupler with optimal \vec{V} , initial \vec{V} , and a conventional directional coupler for $\lambda = 1530 - 1630$ nm. The corresponding $\Delta\beta$ and κ , w_0 , w_1 , and G versus z of the optimal design are shown in Figs. 7(b), (c), (d), (e), and (f), respectively. For the optimal design, P_0 ranges from 49.57% to 50.81% for $\lambda = 1530 - 1630$ nm, hence the power deviation is within ± 0.070 dB and the $\pm 1\%$ bandwidth is in excess of 100 nm, which is up to about 30 times the value in a conventional coupler. Although it is easy to propose a design exhibiting superior performance compared with the conventional directional couplers, the performance of the conventional directional couplers is still a proper benchmark for comparison [10, 15]. By applying the same design method, the optimized design of broadband 75%/25%, 25%/75%, and 0%/100% couplers by the GA are shown in Figs. 8, 9, and 10, respectively. For all cases, the $\pm 2\%$ bandwidths are in excess of 100 nm.

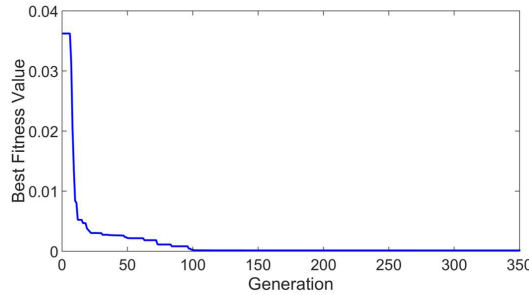


Fig. 6. Evolution of the best fitness value for the generic algorithm.

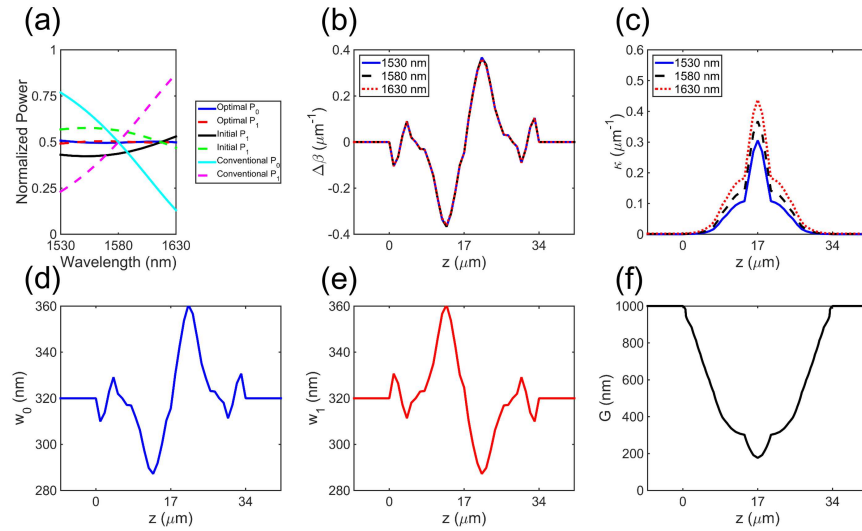


Fig. 7. (a) Normalized power output of the bar and cross ports of the optimal design of a broadband 50%/50% coupler, the initial population, and a conventional directional coupler for the quasi-TM mode where $h = 320$ nm, $\bar{w} = 320$ nm, and $\lambda = 1530 - 1630$ nm. (b) $\Delta\beta$, (c) κ , (d) w_0 , (e) w_1 , and (f) G versus z .

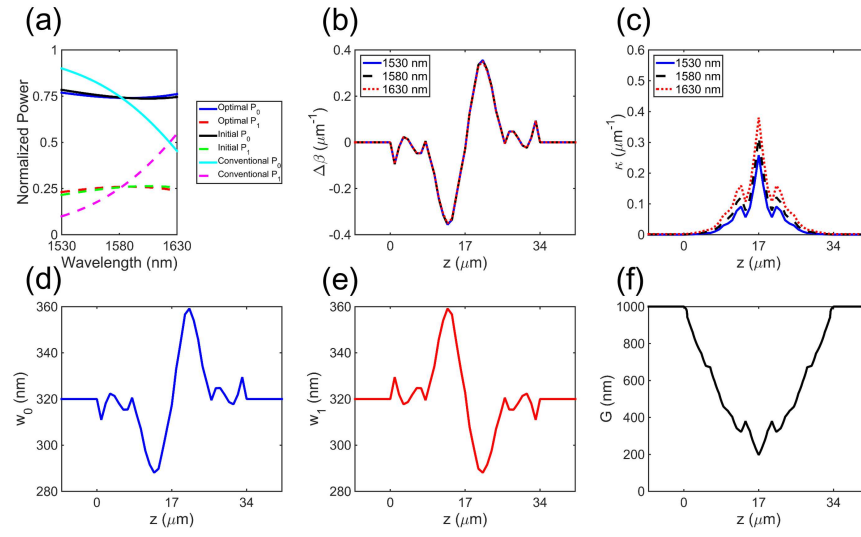


Fig. 8. (a) Normalized power output of the bar and cross ports of the optimal design of a broadband 75%/25% coupler, the initial population, and a conventional directional coupler for the quasi-TM mode where $h = 320\ \text{nm}$, $\bar{w} = 320\ \text{nm}$, and $\lambda = 1530 - 1630\ \text{nm}$. (b) $\Delta\beta$, (c) κ , (d) w_0 , (e) w_1 , and (f) G versus z .

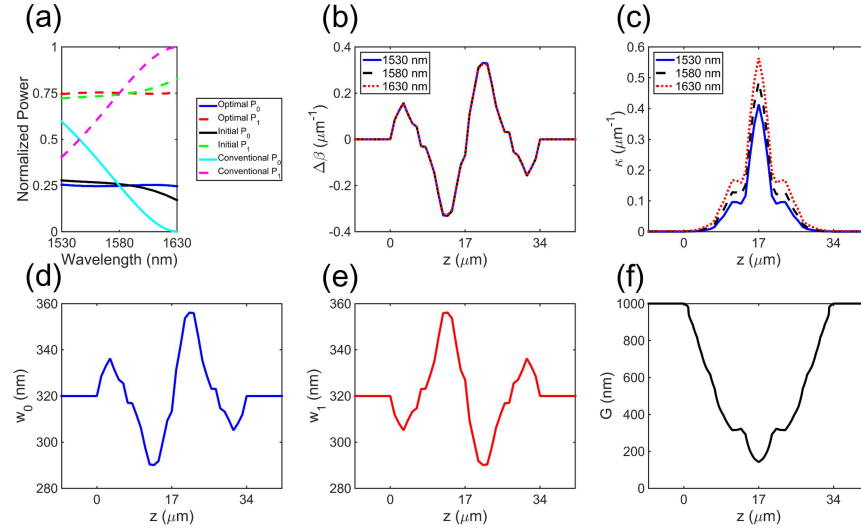


Fig. 9. (a) Normalized power output of the bar and cross ports of the optimal design of broadband 25%/75% coupler, the initial population, and a conventional directional coupler for the quasi-TM mode where $h = 320\ \text{nm}$, $\bar{w} = 320\ \text{nm}$, and $\lambda = 1530 - 1630\ \text{nm}$. (b) $\Delta\beta$, (c) κ , (d) w_0 , (e) w_1 , and (f) G versus z .

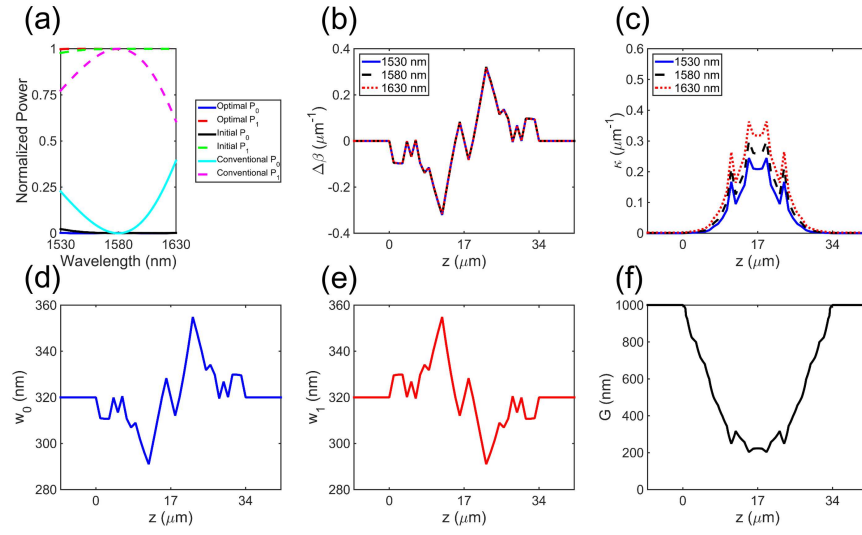


Fig. 10. (a) Normalized power output of the bar and cross ports of the optimal design of a broadband 0%/100% coupler, the initial population, and a conventional directional coupler for the quasi-TM mode where $h = 320$ nm, $\bar{w} = 320$ nm, and $\lambda = 1530 - 1630$ nm. (b) $\Delta\beta$, (c) κ , (d) w_0 , (e) w_1 , and (f) G versus z .

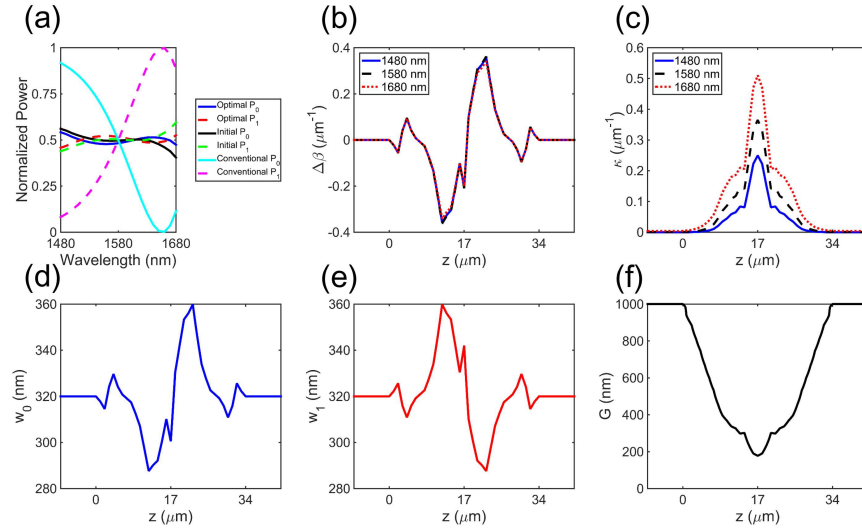


Fig. 11. (a) Normalized power output of the bar and cross ports of the optimal design of a broadband 50%/50% coupler, the initial population, and a conventional directional coupler for the quasi-TM mode where $h = 320$ nm, $\bar{w} = 320$ nm, and $\lambda = 1480 - 1680$ nm. (b) $\Delta\beta$, (c) κ , (d) w_0 , (e) w_1 , and (f) G versus z .

To demonstrate the potential capability of the proposed design concept, a 50%/50% coupler with a bandwidths of 200 nm is designed and optimized. Fig. 11 shows the result, where the power deviation is within ± 0.352 dB.

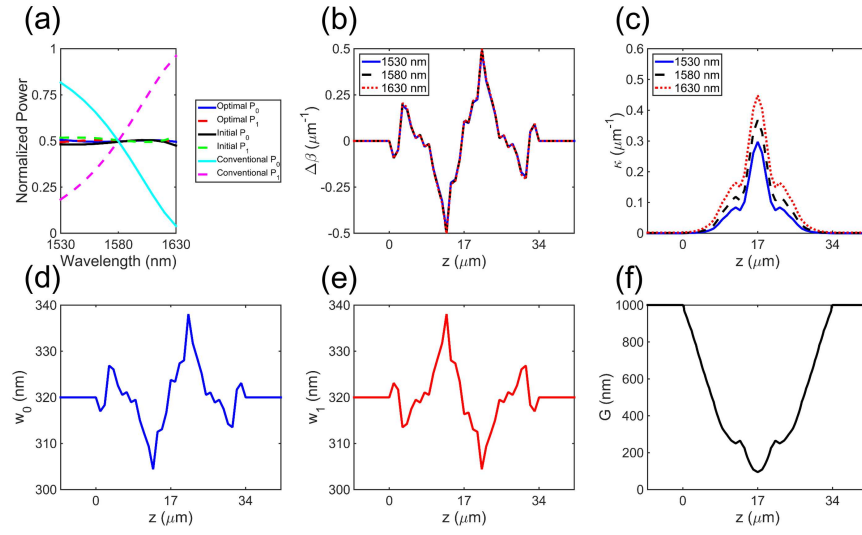


Fig. 12. (a) Normalized power output of the bar and cross ports of the optimal design of a broadband 50%/50% coupler, the initial population, and a conventional directional coupler for the quasi-TE mode where $h = 320 \text{ nm}$, $\bar{w} = 320 \text{ nm}$, and $\lambda = 1530 - 1630 \text{ nm}$. (b) $\Delta\beta$, (c) κ , (d) w_0 , (e) w_1 , and (f) G versus z .

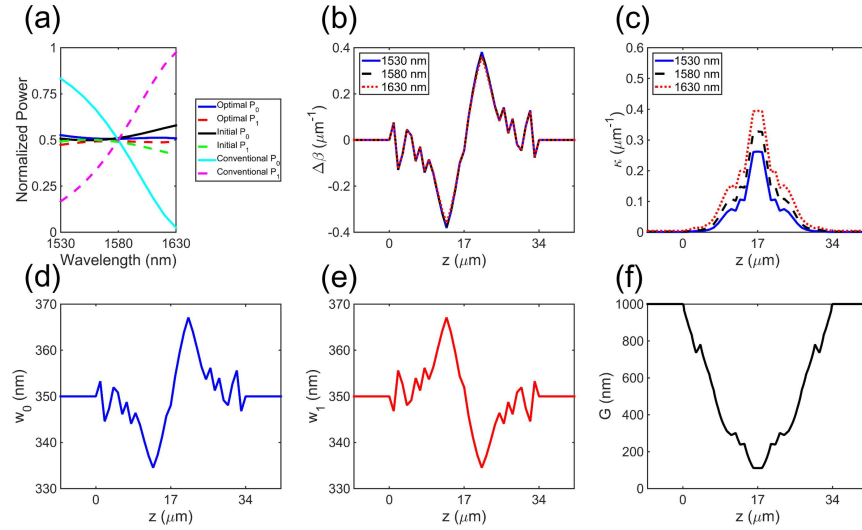


Fig. 13. (a) Normalized power output of the bar and cross ports of the optimal design of a broadband 50%/50% coupler, the initial population, and a conventional directional coupler for the quasi-TE mode where $h = 220 \text{ nm}$, $\bar{w} = 350 \text{ nm}$, and $\lambda = 1530 - 1630 \text{ nm}$. (b) $\Delta\beta$, (c) κ , (d) w_0 , (e) w_1 , and (f) G versus z .

Once a specific case is optimized, the result can be a starting point of the initial design for other cases with arbitrary waveguide geometry, polarization, even central wavelength but with identical device length and target coupling ratio. Since we have obtained an optimized case of a 50%/50% coupler for quasi-TM mode with $h = \bar{w} = 320 \text{ nm}$, identical κ and $\Delta\beta$ in the

z -direction for quasi-TE mode with arbitrary h and \bar{w} should lead to the same result. The design dimensions including w_0 , w_1 , and G can be obtained from the newly built lookup table which can be set as the initial population for the next optimization process for conveniency. The optimal design of 50%/50% couplers for the quasi-TE mode with $(h, \bar{w}) = (320 \text{ nm}, 320 \text{ nm})$ and $(h, \bar{w}) = (220 \text{ nm}, 350 \text{ nm})$ are shown in Figs. 12 and 13, and the power deviations are $\pm 0.055 \text{ dB}$ and $\pm 0.222 \text{ dB}$, respectively.

4. BEM simulation

Although the optimal design can be analyzed by the CMT, the approximated κ is used and the propagation direction is not exactly parallel to the z -axis. This may cause errors to arise in some cases. To verify the accuracy of the design, a numerical simulation containing the geometry constructed by the resultant \vec{V} optimized by the GA is needed. In this case, the full-vectorial BEM (similar to the FEBPM) is used where the electric field is composed of a slowly varying envelope term and a rapidly varying phase term. The full-vectorial BEM simulation takes all components in the x , y , and z -direction for the electric and magnetic fields into account, and we believe that the simulation results are sufficiently accurate to verify the results calculated by the transfer matrix method used in the optimization process. On the premise that the major propagation direction is well-defined, the BEM enables accurate simulations of optically large systems without the requirement of very fine meshes much smaller than λ [27]. Also, a simulation based on the 2D-FEM is performed for verification, because large computational efforts are required in real 3D simulation based on the FEM. The 2D equivalent structure is built by the in-house developed method and similar method has been widely used in the commercial software with sufficiently accurate results [33]. More detailed information for the 2D equivalent structure is given in [34].

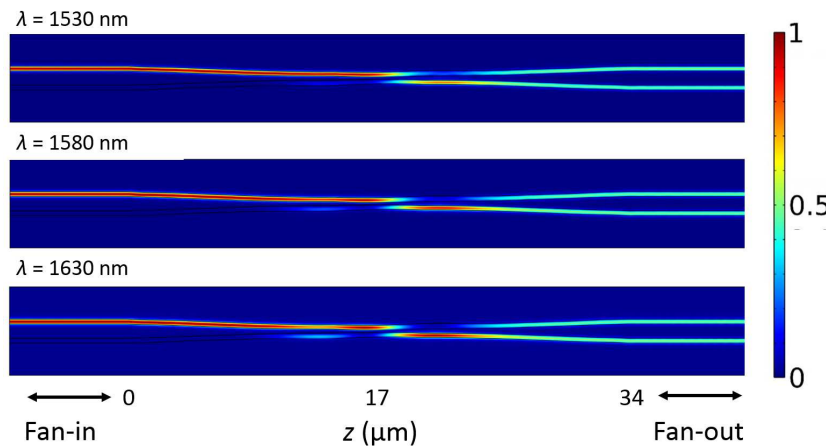


Fig. 14. Normalized optical power distribution fields of the optimal design for $\lambda = 1530$, 1580, and 1630 nm.

Figure 14 shows the normalized optical power distribution fields of the optimal design for $\lambda = 1530$, 1580, and 1630 nm, which represent the short, medium, and long wavelengths, respectively, in the target range for $\lambda = 1530$ –1630 nm. The result shows good agreement with the CMT where the coupling ratios of the bar and cross ports are very close to 50%/50% for all three wavelengths. The coupling depth and the periodicity can be designed by optimizing κ and $\Delta\beta$ of each section and thus the wavelength dependency can be significantly reduced compared with conventional couplers. Figure 15 presents the coupling ratio of the bar port, P_0 , and the cross port, P_1 for $\lambda = 1500$ –1660 nm calculated by the CMT, BEM, and the FEM. The difference is less

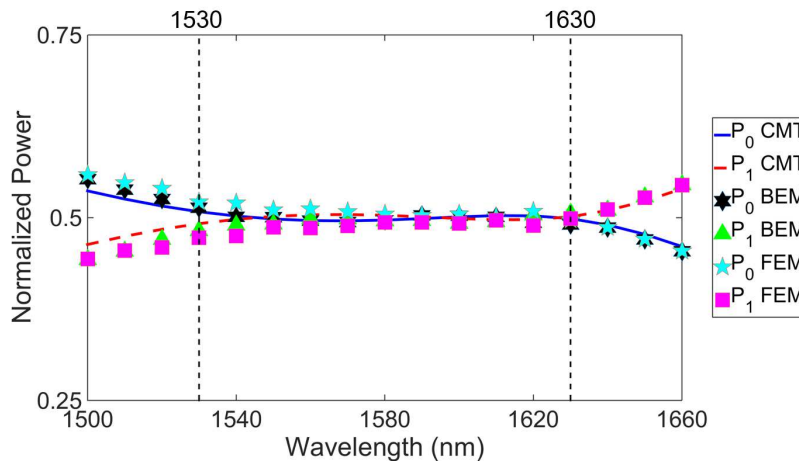


Fig. 15. P_0 and P_1 versus wavelength for $\lambda = 1500\text{--}1660\text{ nm}$ calculated by the CMT, BEM, and FEM

than 1% for $\lambda = 1530\text{--}1630\text{ nm}$ and 2% for $\lambda = 1500\text{--}1660\text{ nm}$ between the results simulated by the CMT and BEM. The results of the FEM also show good agreement with the CMT, but the deviation is a bit larger compared with the BEM. Although Si and SiO_2 are lossless in the range of the target wavelengths, the CMT ignores the light power leakage and slight reflections when the geometry of the waveguides vary as the light propagates. The total normalized output power $P_0 + P_1$ is 99.2%–99.7% for the BEM or the FEM while it is equal to unity for the CMT calculations. Owing to the restrictions of the variables during the optimization process, the CMT analysis is generally accurate in this case. It is pertinent to mention that the calculation time for $\lambda = 1580\text{ nm}$ is in the region of 495 seconds for the BEM, 245 seconds for the FEM but is about 0.006 seconds for the CMT analysis. Therefore, to complete the design in a reasonable time, the CMT analysis is a good choice for the optimization that handles a wide variety of variable combinations and the BEM or the FEM can be used to verify the accuracy of the CMT.

5. Fabrication tolerance analysis

Figure 16 shows P_0 and P_1 versus Δw for $\lambda = 1530, 1580$, and 1630 nm calculated by the CMT where Δw is the fabrication error for the waveguide widths, and the positions of the centers of WG0 and WG1 remain the same regardless of Δw . In this case, Δw is assumed constant for all the waveguide widths or shapes along the device. Note that the result may be different if Δw is not a constant across the entire wafer. Figures 17(a) and (b) respectively shows $\Delta\beta$ and κ versus z at $\lambda = 1580\text{ nm}$ for different values of Δw . The variation of Δw results in a slight change of $\Delta\beta$. On the other hand, κ is nearly independent of Δw . The increase of Δw may result in a decreased G , and κ can be compensated by the two mechanisms that occur simultaneously. The decrease of G may result in an increased κ while the increase of Δw may result in an increased optical confinement in the silicon strip and thus a decreased κ [15]. The fabrication tolerance can be further improved by reducing the sensitivity of $\Delta\beta$ to λ , and the most straightforward ways are increasing \bar{w} or using a material with a lower refractive index compared with Si, such as SiN, but larger h or \bar{w} may required as well.

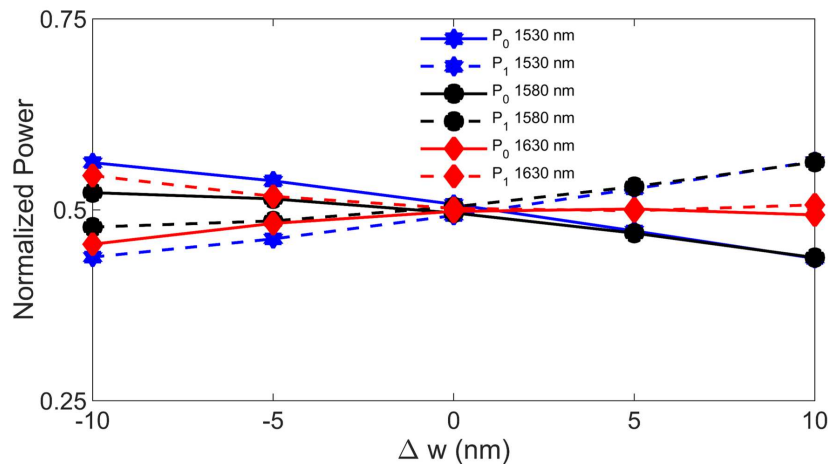


Fig. 16. Fabrication tolerance versus Δw for $\lambda = 1530, 1580$, and 1630 nm.

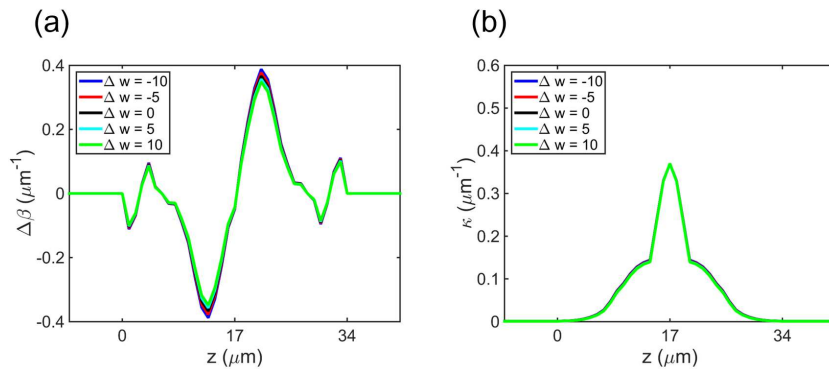


Fig. 17. (a) $\Delta\beta$ and (b) κ versus z at $\lambda = 1580$ nm for different values of Δw .

6. Conclusion

In summary, this study proposes the optimization of broadband optical waveguide couplers for arbitrary coupling ratios on a silicon photonic platform based on a GA. The deviation of coupling ratios is less than 2% for 75%/25%, 50%/50%, 25%/75%, and 0%/100% couplers for $\lambda = 1530 - 1630$ nm (i.e., over the C + L band). The sensitivity of the coupling ratio to λ variations can be suppressed by optimizing the waveguide geometry of each section. Moreover, the system can be analyzed by the CMT in the form of transfer matrices, and the result agrees well with the numerical simulations based on the BEM. To our knowledge, this is the first design of a broadband optical waveguide coupler carried out by a GA by segmenting the whole device into short sections. The device is found to have excellent performance, and the design concept will benefit the development of silicon photonic technology.

Funding

Ministry of Education, Taiwan, R.O.C. (104R890958); Ministry of Science and Technology, Taiwan, R.O.C. (MOST) (103-2221-E-002-060).